Investigating Cases of Jump Phenomenon in a Nonlinear Oscillatory System

Hamid A. Ardeh(⊠)
Department of Mechanical Engineering
University of Wisconsin-Madison
Email: ansariardeh@wisc.edu

Matthew S. Allen
Department of Engineering Physics
University of Wisconsin-Madison
Email: msallen@engr.wisc.edu

Abstract

A two degree-of-freedom (DOF) nonlinear oscillatory system is presented which exhibits jump phenomena where the period of oscillation jumps to an integer multiple of its original period when the state changes by a small amount due to damping. The jump phenomenon is investigated within the framework of Catastrophe theory where the abrupt change in the response characteristic of the system is explained by the interaction between its invariant manifolds. The authors recently presented an approach based on the concept of the Instantaneous Center Manifold (ICM), where, the center manifold of a conservative nonlinear system was replaced by an equivalent set of ICMs as two-dimensional invariant manifolds of the system that contain all of its periodic orbits. This study attempts to explain the sudden change in the response of a slightly damped oscillator as its response decays, based on the ICMs of its underlying undamped system. Such abrupt changes in the response of the system are explained based on the orientability properties of the local ICMs of the undamped system. This study also presents a bifurcation analysis of periodic orbits of the undamped system to illustrate the evolution of different types of periodic orbits, orientability of their local ICMs and their effect on the transient response of the damped system. These effects are expounded in cases of jump phenomena observed in numerical simulation of the free response of the damped system.

Keywords: Jump Phenomena, Instantaneous Center Manifold, Nonlinear Mode, Orientability, Bifurcation Theory, catastrophe Theory

1 Introduction

Mechanical systems often exhibit phenomena in which the response of the system changes character dramatically for a seemingly small change of some parameter. These phenomena are often characterized by a large amplitude discontinuity in the dynamic response of the system to small amplitude disturbances. Some examples include; sudden jumps in nonlinear torsional vibration of a power transmission system [1], vibration of nonlinear dynamic absorbers [2, 3, 4], forced vibration of a diaphragm air spring [5, 6], dynamic oscillation of a diesel generator [7], forced vibration of bladed disks (internal resonance)[8, 9, 10], roll-coupled maneuvers of airplanes [11, 12, 13] and vibration of mechanical and electrical systems described by Duffing's equation [14, 15, 16, 17]. Standard perturbation methods such as Poincare-Linsteddt method and multiscale method, which are most suited for approximation of small amplitude nonlinear responses, can not be used to describe the large amplitude associated with such discontinuities. In these cases, catastrophe theory provides a natural synthesis between the practically observable and theoretical aspects of their sharp discontinuity when a small continuous change is made.

Catastrophe theory originated in the mid-1960's, with the ideas of French topologist Thom which were published in the book [18]. Later, Zeeman [19] suggested that the theory of catastrophes, to mean a particular mathematical model of catastrophic changes in the response of a system, should be called "Catastrophe Theory". The centerpiece of Catastrophe theory is Thome's transversality theorem. This theorem asserts that two manifolds, in general position, intersects transversely where the intersection is stable in a sense that a small perturbation will not change the nature of the response significantly. However, when the intersection

is non-transversal, any arbitrarily small perturbation will change the qualitative nature of the intersection dramatically. One can determine whether an intersection is transverse by checking the Jacobian of the manifolds at the intersection. What can be defined as the manifolds, in Thom's transversality theorem, depends on the response characteristic of the system being studied. If the solution of the system in state space is being investigated, one can choose the stable, unstable and center manifolds of the system as the invariant manifolds in Thom's transversality theorem.

However, for conservative oscillatory systems, the invariant manifolds of the system reduce down to only the center manifold which is, in general, defined in a high dimensional space. In a recent study, Ardeh et al [20], using the center manifold theory, proposed an approach to replace the center manifold with an equivalent set of low dimensional invariant manifolds which were named Instantaneous Center Manifolds. Later, following the works of Rosenberg [21, 22, 23, 24, 25], Shaw et al [26, 27, 28] and Kerschen et al [29, 30], the ICM concept was used to define nonlinear modes of vibration as periodic orbits on these invariant manifolds of the system. This definition, not only extended the previously defined set of invariant manifolds of fixed points by Shaw et al [26, 27, 28] to include the invariant manifolds of periodic obits, but was also capable of capturing the entire geometry of such manifolds (see [31] for more details).

These recently discovered invariant manifolds of periodic orbits, in a sense, are more significant than those associated with the fixed points of the system, since they intersect with the manifolds of fixed points non-transversely. That is because, at the point where they intersect the manifolds of the fixed points, the Jacobian of the center manifold is singular. This condition, i.e. singularity of the Jacobian of the center manifold, is often called the (internal) resonance condition where DOF of the system oscillate at unequal frequencies with rational ratios.

Moreover, as it will be discussed in Section 5, periodic orbits on the new interconnecting manifolds are products of bifurcations of periodic orbits on the invariant manifolds of fixed points, i.e. the manifolds of the primary nonlinear normal modes discussed in [29]. In this sense, since catastrophes are bifurcations between different equilibrium or fixed point attractors, these new interconnecting manifolds can be used to explain unexpected phenomena such as jump phenomena. In other words, one may roughly define Catastrophe theory "Bifurcation theory from the topological viewpoint" that is the study from a qualitative point of view of the ways that solutions to differential equations change [32, 33, 34]. The inverse relation has been previously studied by Arnold [35] where Thom's transversality theorem was used to locate bifurcations in versal families[1]. In this regard, this study attempts to explain catastrophes, observed in a case study, by establishing a connection between Bifurcation theory and Catastrophe theory through the concepts of ICMs and nonlinear modes of vibration.

To this end, Section 2 presents a two DOF conservative nonlinear system. The ICMs of the systems are calculated and illustrated in different views, each, emphasizing a different characteristic of the periodic orbits of the system. The concept of orientability is discussed in Section 3 to explain how it affects the evolution of the transient response of a dynamical system. Moreover, examples of orientable and non-orientable local ICMs of the conservative 2DOF system are presented. Section 4 discusses the stability of periodic orbits of the system in question and the relation between the stability of periodic orbits and orientability of their local ICMs. In addition, this section presents presents the upper limit of the approximation error in calculating the Floquet exponents. This limit defines a criteria that can validate the calculated Floquet exponents in stability analysis of periodic orbits, , and is the key to accurately assessing the stability of the orbits studied here. This section also explains the mechanisms of losing stability, through which, some of the less trivial periodic orbits of the system bifurcate from other equilibria. In Section 5, the conservative system is modified by adding very small damping terms which are treated as perturbation terms. This is used to study the effect of changing changing the damping terms on the free response of the system, especially in the cases of jump phenomena. This study reveals that the jump phenomena occur as the state of the system approaches local manifolds with different orientability properties. Conclusions and directions for future work are provided in Section 6.

[1] A set of deformations that retains a special universal property under certain changes.

2 Case Study: The Underlying Conservative System

In this section, the two DOF conservative, nonlinear oscillatory system, shown in Fig.1, is considered. The periodic orbits of the systems are calculated and illustrated in three different views; an invariant manifold (ICM) representation, an energy-frequency plane representation and a cross-section view of their Poincare map.

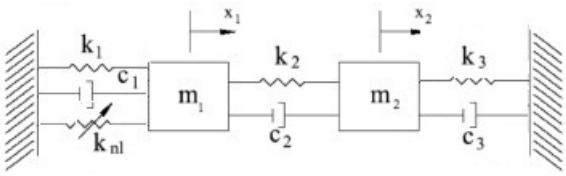

Figure 1: A two DOF nonlinear oscillatory system.

Equations of motion (EOM) for the system shown in Fig.(1) can be obtained for the following parameters values $k_1 = k_2 = k_3 = 1$, $c_1 = c_2 = c_3 = 0$ and $k_{nl} = 0.5$ as

$$\begin{bmatrix} \ddot{x}_1 \\ \ddot{x}_2 \end{bmatrix} = -\begin{bmatrix} 2 & -1 \\ -1 & 2 \end{bmatrix} \begin{bmatrix} x_1 \\ x_2 \end{bmatrix} - \begin{bmatrix} 0.5x_1^3 \\ 0 \end{bmatrix}, \tag{1}$$

which can also be recast in state space defined by $(x_1, x_2, y_1, y_2) = (x_1, x_2, \dot{x}_1, \dot{x}_2)$ as

$$\begin{bmatrix} \dot{x}_1 \\ \dot{x}_2 \\ \dot{y}_1 \\ \dot{y}_2 \end{bmatrix} = \begin{bmatrix} 0 & 0 & 1 & 0 \\ 0 & 0 & 0 & 1 \\ -2 - \frac{3}{2}x_1^2 & 1 & 0 & 0 \\ 1 & -2 & 0 & 0 \end{bmatrix} \begin{bmatrix} x_1 \\ x_2 \\ y_1 \\ y_2 \end{bmatrix}. \tag{2}$$

2.1 Periodic Orbits in the Energy-Frequency Plane

One of the characteristic features of nonlinear systems is the frequency-energy dependence of their periodic orbits (nonlinear modes). As a result, the modal amplitudes and frequencies of nonlinear modes depend on the total energy of the system. Regarding this dependence, one typical representation of nonlinear modes is an energy-frequency plot. In this plot, a branch of nonlinear modes, which represents an invariant manifold (ICM), qualitatively shows how the frequencies of periodic orbits change as the total energy of the system increases. In this regard, the (scaled) frequencies of the periodic solutions of the system (1) are shown as functions of their their energy in Fig 2. The scaled frequency f_s is defined as

$$f_s = \begin{cases} f & \text{ICM I and ICM II} \\ \frac{1}{f_{max} - f_{min}} \left[m(f - f_{min}) - n(f - f_{max}) \right] f & \text{Otherwise} \end{cases} \tag{3}$$

where f is the fundamental frequency of periodic orbits of the system (1), and m and n are the positive integer factors in the terms ICM I-m, II-n referring to an invariant manifold (ICM) that intersects with the ICM I and ICM II at periodic orbits that are cases of, respectively, m:1 (m to one) and n:1 resonances, i.e. $f_1 = mf_2$ and $f_1 = nf_2$. It is important to notice that the frequency f_s represents the fundamental frequency only for the ICM I and ICM II. For all of the other ICMs, f_s represents a scaled version of their fundamental frequencies, where, the scaling factor is a positive integer only at the intersection of theses ICMs with the ICM I and ICM II. This scaling is done to show all of the branches of the nonlinear modes in a region between the two branches defined by ICM I and ICM II.

2.2 Periodic Orbits on the Invariant Manifolds of the System

Periodic orbits of the system (1) are found using the ICM approach and continuation algorithm [31, 30] and used to construct the ICMs of the system (1). Examples of such ICMs are shown in Fig. 3. Each manifold

is constructed by creating a mesh in which each individual solution, i.e. a periodic orbit (limit cycle) of the system (1), generates a tray of the geometry of the invariant manifold.

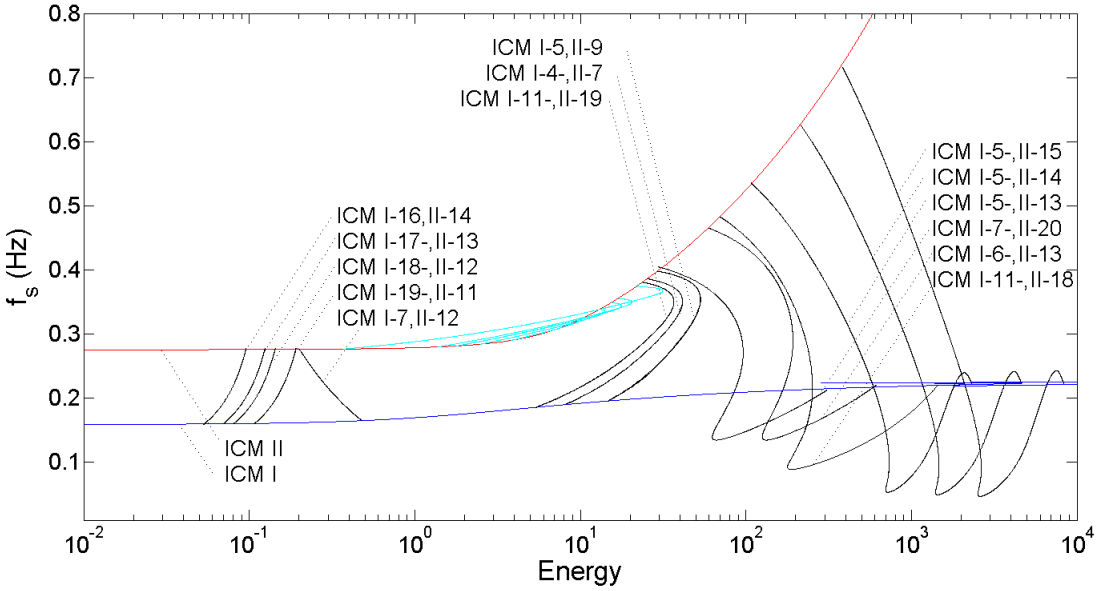

Figure 2: Scaled frequencies of periodic orbits nonlinear modes on ICMs are shown as functions of their energies for the same ICMs. Scaled frequencies are calculated using Eq. (3). One group of ICMs, shown in cyan, start from the ICM II and land on ICM II while the other group of ICMs, shown in black, start from the ICM I (ICM II) and land on ICM II (ICM I).

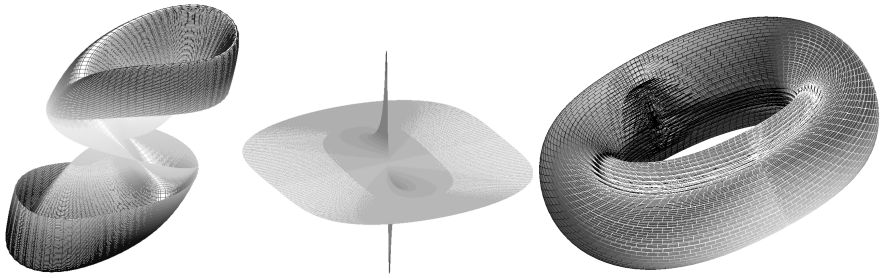

Figure 3: The displacement components of some of the ICMs are shown. For each surface, x_2 of the system is plotted versus the x_1 and H_{x_1} where x_1 is the first DOF chosen as the independent variable and H_{x_1} is the Hilbert transform of x_1. Left: First (of two) invariant manifolds that is tangent to the vector field of the system at its fixed point, i.e. the origin. Middle: Second invariant manifold that is tangent at the fixed point of the system. Right: One of infinitely many invariant manifolds that is tangent to the vector field of the system at its periodic orbit. This manifold is an example of one that connects the other two invariant manifolds, as mentioned in Section 1.

2.3 Periodic Orbits as Fixed Points of a Poincare Map

Another way to illustrate the periodic orbits of this system is through a Poincare map. In this regard, a Poincare section Ω is defined by $\Omega = \{(x_1, x_2, y_1, y_2) \in \mathbb{R}^4 | y_2 = 0\}$. The set Ω defines a hyperplane in $\mathbb{R}^4$which

has the property that all the solutions of the system in (2) cross it transversely. This can be validated by proving that the tangent on the solutions of the system (2) when they cross this hyperplane, i.e.

$$\frac{d}{dt}\begin{bmatrix} x_1 \\ x_2 \\ y_1 \\ y_2 \end{bmatrix}_{y_2=0} = \begin{bmatrix} \dot{x}_1 \\ \dot{x}_2 \\ \dot{y}_1 \\ \dot{y}_2 \end{bmatrix}_{y_2=0} = \begin{bmatrix} 0 & 0 & 1 & 0 \\ 0 & 0 & 0 & 1 \\ -2-\frac{3}{2}x_1^2 & 1 & 0 & 0 \\ 1 & -2 & 0 & 0 \end{bmatrix} \begin{bmatrix} x_1 \\ x_2 \\ y_1 \\ y_2 \end{bmatrix}_{y_2=0} = \begin{bmatrix} y_1 \\ 0 \\ -2x_1 + x_2 - \frac{3}{2}x_1^3 \\ x_1 - 2x_2 \end{bmatrix}, \quad (4)$$

is non-zero. One can readily show that the tangent vector (4) is almost always non-zero, except at the origin which is the fixed point of the system (1). Next, a cross-section of fixed points of the mentioned Poincare map defined by the plane $y_1 = 0$, a contour of the Poincare map, is shown in Fig. 4. In addition, fixed points in this cross-section of the Poincare map are shown for varying f_s in Fig.5 where three groups of ICMs can be recognized. First, denoted by ICM I and ICM II, are the loci of all the nonlinear modes (periodic orbits) that are continuations of linear modes of the system. Second, shown in cyan, is a group of ICMs that resemble contours of two saucer-shape surfaces sitting on top of the ICM II. The last group consists of two types of ICMs; a saddle-shape and a group of inverted saddle-shape ICMs. The last two groups are products of bifurcations from the periodic orbits (modes) on ICMs I and II. This will be further investigated in Sections 4 and 5.

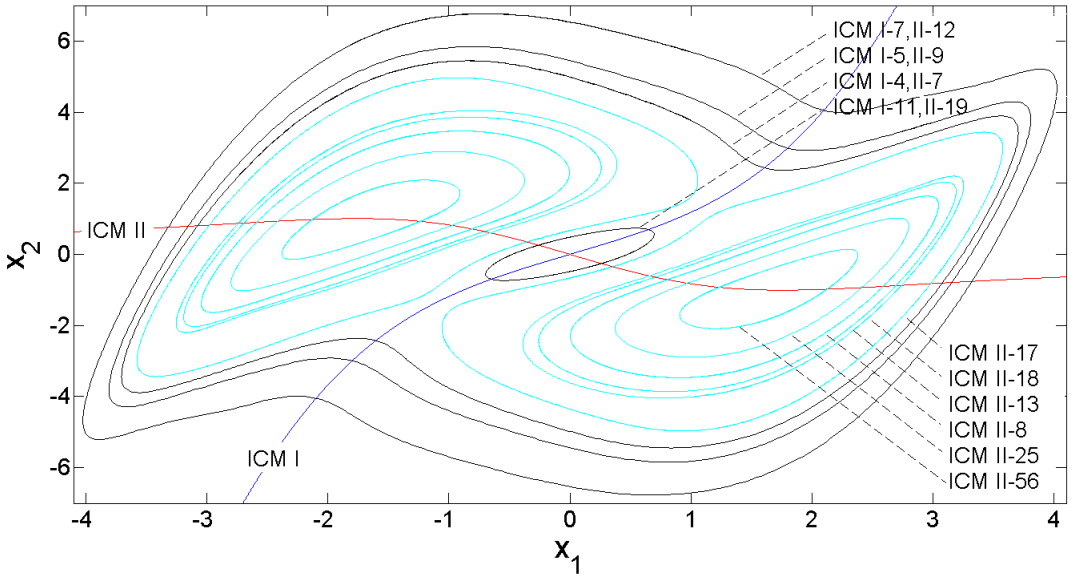

Figure 4: Cross-section of a Poincare map is shown for the solutions with energies less than 35. Other than ICM I and ICM II, which are the loci of all the linear modes and their nonlinear continuations two other groups of ICMs are identified. First, shown in cyan, is a group of ICMs that only cross the ICM II. The second group, shown in black, consists of ICMs that cross both ICMs I and II.

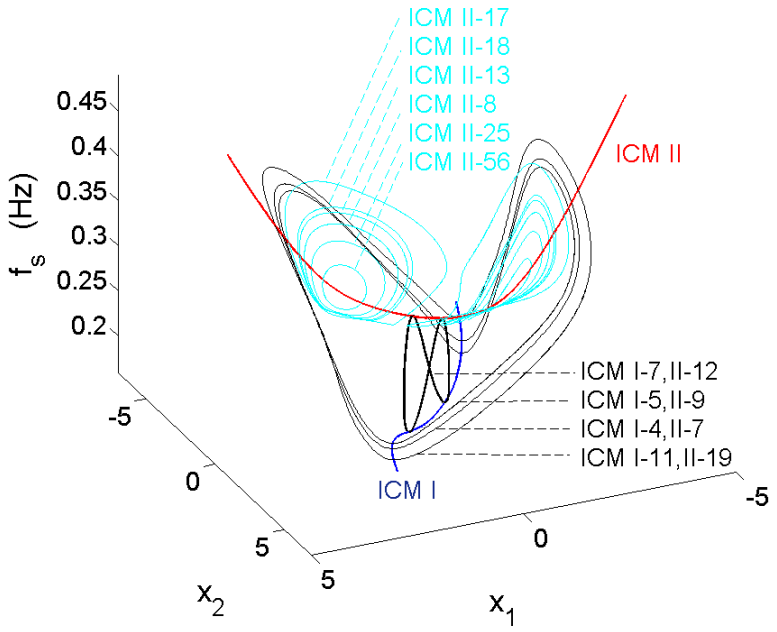

Figure 5: Scaled frequencies of periodic orbits on ICMs are shown versus the fixed points of the Poincare map.Scaled frequencies are calculated using Eq. (3).

3 Orientability of Invariant Manifolds

To understand the dynamics of conservative vector fields, one typically looks for attractors (stable limit cycles or periodic orbits), their basin of attraction and, in particular, the boundaries of these attracting domains. Invariant manifolds often act as basin boundaries, and it is important to know where they are located and what they look like [36, 37]. These manifolds are sometimes called separating manifolds, as they separate the state space into two invariant regions. Orbits starting on one side of the manifold are confined to this region since they cannot pass through an invariant manifold. In particular, a separating manifold must have two sides, namely an inside and an outside. However, there are two-dimensional invariant manifolds that do not have two sides. Such manifolds are called nonorientable manifolds.

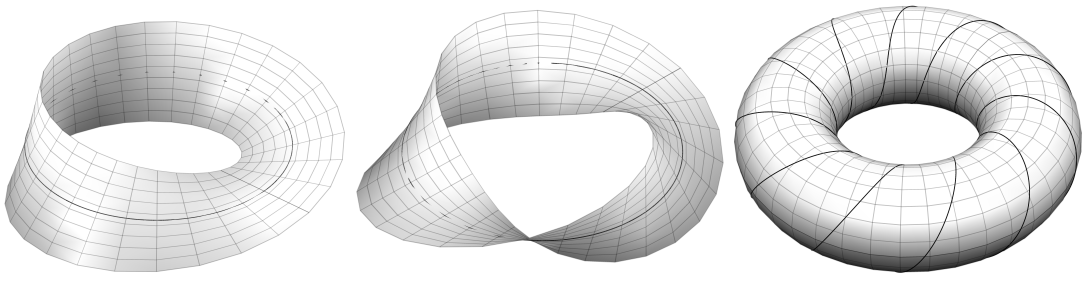

Figure 6: Left: The Mobius strip is a nonorientable surface. Middle: A twisted strip represents an orientable surface. Right: Torus is also an orientable surface.

The classical example of a nonorientable manifold is the Mobius strip. A Mobius strip can be easily made by wrapping a strip of paper around a circle and gluing its ends together after giving it half of a twist (see

Fig. 6). This surface only has one side since any trajectory that starts on the top surface will end up on the opposite surface after one cycle. In other words, orbits can advance through this type of surface without crossing it. Two examples of orientable surfaces, i.e. a twisted strip and a torus, are also shown in Fig. 6. Orbits that starts on one side of the twisted strip or inside of a torus can not move through these surfaces without crossing them.

The Mobius strip is the only two dimensional non-orientable manifold that can be embedded in $\mathbb{R}^3$ without self-intersection. For example, for the system in 1, the local invariant manifolds of the period lengthened periodic orbits form complicated manifolds that intersect themselves. However these manifolds, a few of which are shown in Fig. 7 are nonorientable and have very similar structures to that of the Mobius strip. The complexity of these manifolds is caused by the shape of their periodic orbits (mode shapes). In other words, to construct theses manifold, like the Mobius strip, one can start with a strip of paper but, in this case, the strip needs to be wrapped along the mode shape of the periodic orbit instead of a circle. Also, its ends now need to be glued together after an odd number of half twists.

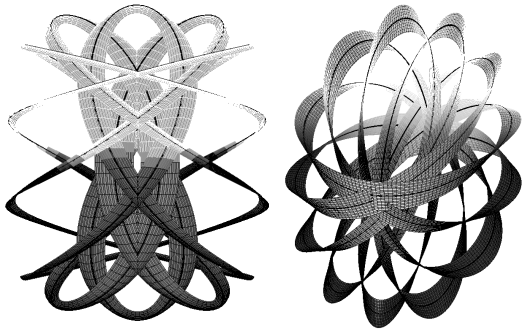

Figure 7: Examples of nonorientable manifolds. Left: A local ICM representing a twisted strip with $(5+8)\times\frac{1}{2}$ (thirteen half) twists around a periodic orbit, shown with a solid black line, with 5:8 resonance. Right: A local ICM representing a twisted strip with $(16+1)\frac{1}{2}$ (seventeen half) twists.

The system (1) also has several periodic orbits along orientable manifolds. For example, Fig. 8 represents three cases of twisted strips with, respectively, one, four and six full twists and a case of a torus local ICM.

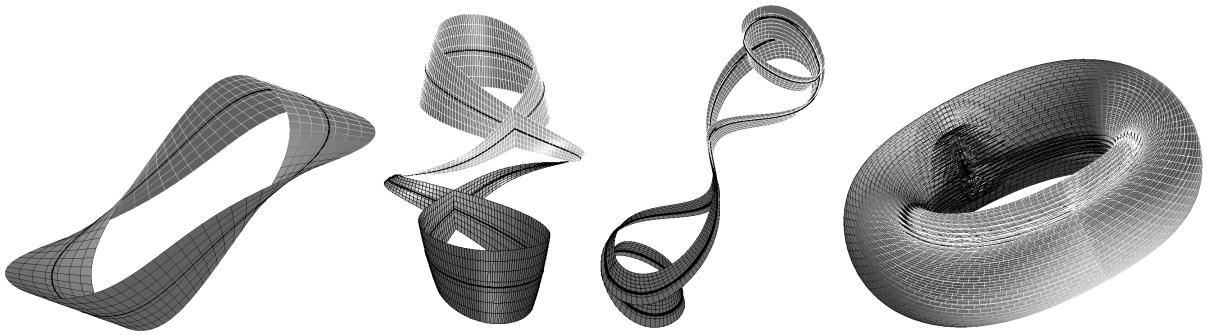

Figure 8: Examples of orientable manifolds. Left: A local ICM representing a twisted strip. Middle-Left: Local ICM of a periodic obit with 3:1 resonance. This surface can be made by wrapping a strip of paper along the mode shape of the periodic orbit, shown in black, and gluing its ends after $(3+1)\times\frac{1}{2}$ twists. Middle-Right: Local ICM of a periodic obit with 5:1 resonance. Right: A torus local ICM.

These local invariant manifolds are key building blocks in shaping the orbits of nonlinear conservative systems, since, they can be seen as the gates and walls of the state space that the orbits of these systems can move through and cannot cross, respectively. In this regard, one needs a quantitative tool to determine the orientability (or nonorientability) of these local ICMs. This can be done through the stability analysis of their corresponding periodic orbits.

4 Stability of Periodic Orbits and Orientability of Their Invariant Manifolds

In this section, the relation between the orientability of local ICMs and the stability of their defining periodic orbits is explained. In order to determine the stability of periodic orbits of nonlinear systems, one needs to perform a Floquet analysis. In this regard, Floquet theory is explained briefly next.

4.1 Stability of Periodic Solutions (Floquet Theory at a Glance)

Stability of periodic solutions of nonlinear system is assessed by analyzing the boundedness or otherwise of the solutions of the linearization of the system around its periodic orbit. In this sense, considering a n DOF nonlinear, conservative system defined by

$$\dot{\boldsymbol{z}} = \begin{bmatrix} \dot{\boldsymbol{x}} \\ \dot{\boldsymbol{y}} \end{bmatrix} = \begin{bmatrix} \boldsymbol{y} \\ \boldsymbol{f}(\boldsymbol{x}) \end{bmatrix} = \boldsymbol{F}(\boldsymbol{z}) \tag{5}$$

with a periodic solution represented by $\bar{\boldsymbol{z}} = [\bar{\boldsymbol{x}}^T, \bar{\boldsymbol{y}}^T]^T$, Floquet theory replaces (5) with its linear approximation about the periodic solution $\bar{\boldsymbol{z}}$

$$\dot{\boldsymbol{z}} = \begin{bmatrix} \dot{\boldsymbol{x}} \\ \dot{\boldsymbol{y}} \end{bmatrix} = \begin{bmatrix} \boldsymbol{0} & \boldsymbol{I} \\ \mathbb{J}_{\boldsymbol{f}}(\bar{\boldsymbol{x}}) & \boldsymbol{0} \end{bmatrix} \begin{bmatrix} \boldsymbol{x} \\ \boldsymbol{y} \end{bmatrix} = \mathbb{J}_{\boldsymbol{F}}(\bar{\boldsymbol{z}})\boldsymbol{z},\ i,j = 1,...,n, \tag{6}$$

and studies the boundedness of its solutions in order to determine the stability of the periodic solution of the original nonlinear system.

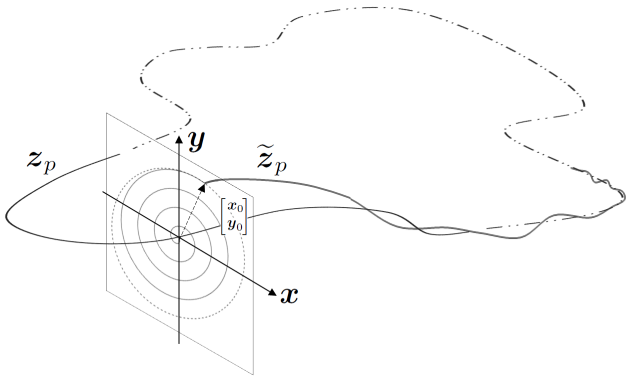

Figure 9: Floquet theory essentially replaces the nonlinear system by its corresponding linear system at each point along the periodic solution. The perturbed periodic solution $\widetilde{\boldsymbol{z}} = \bar{\boldsymbol{z}}(t*+T) + \begin{bmatrix} \boldsymbol{x}_0 \\ \dot{\boldsymbol{x}}_0 \end{bmatrix}, \begin{bmatrix} \boldsymbol{x}_0 \\ \dot{\boldsymbol{x}}_0 \end{bmatrix} \lll \bar{\boldsymbol{z}}(t*+T)$, where $\bar{\boldsymbol{z}}(t*+T)$ represent an arbitrary point along the periodic solution $\bar{\boldsymbol{z}}$ and $\begin{bmatrix} \boldsymbol{x}_0 \\ \dot{\boldsymbol{x}}_0 \end{bmatrix}$ is the perturbation term, will asymptotically converge (will not diverge) to the periodic solution $\bar{\boldsymbol{z}}$ if the solution of linear system (6) is stable (marginally stable), i.e. the response to the perturbation term is bounded.

Since $\bar{\boldsymbol{z}}$ has a period T, so does the Jacobian matrix $\mathbb{J}_{\boldsymbol{F}}(\bar{\boldsymbol{z}})$ and based on Floquet theory, solutions of the (6) accept the form

$$e^{\mu t}\boldsymbol{p}(t) \tag{7}$$

where $\boldsymbol{p}(t)$ is also periodic with period T. This way, Floquet concluded that the solutions of the linear system (6) are bounded, and consequently the periodic solution of the nonlinear system (5) is stable, if for all the Floquet exponents μ_i, $\mathtt{Re}\{\mu_i\} \leq 0$, $i = 1,...,2n$.

In order to calculate the Floquet exponents of the system (6) one may first find its characteristic multipliers. Denoting the fundamental matrix of the system in (6) by $Z(t) = \left[\boldsymbol{z_1} \vdots \cdots \vdots \boldsymbol{z}_n\right]$, where $\boldsymbol{z_1}, ..., \boldsymbol{z}_n$ are n linearly independent solutions of the system (6), the characteristic multipliers of the system (6), i.e. $\rho_1, ..., \rho_n$, can be defined as the eigenvalues of the monodromy matrix

$$B = Z(0)^{-1} Z(T). \tag{8}$$

The characteristic exponents or Floquet exponents of the system (6) are then defined as $\mu_1, ..., \mu_n$ satisfying

$$e^{\mu_i T} = \rho_i. \tag{9}$$

Figure 10 shows the Floquet exponents of the system (1) for the ICMs I-11,II-19 and II-2. All regions with at least one positive Floquet exponent represent unstable periodic orbits.

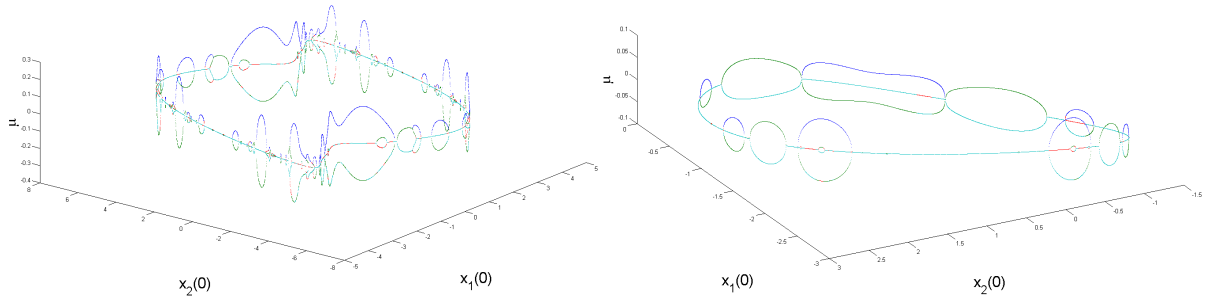

Figure 10: Real parts of Floquet exponents are shown for the ICMs I-11,II-19 (left) and II-25 (right) over the cross-section of the Poincare map defined in Section 2. When one or more exponent is positive, the corresponding periodic orbit is unstable.

4.1.1 Range of Validity of Floquet Stability Analysis

As mentioned above, the stability of the periodic solution of (5) is evidenced by (the signs of) the (largest) Floquet exponents of its associated linear system. Frequently, the eigenvalues computed based on a numerical solution to Eq (6) are not accurate enough to allow stability to be assessed as clearly as is shown shown in Fig. 10. That is because, the periodic solution of the original nonlinear systems (5), its period and also the solutions of its associated linear system used in (8) are all prone to approximation error. Therefore, in order to assure the validity of the stability analysis, one has to show that all the aforementioned sources of approximation errors would lead to an acceptable error $|\delta Re\{\mu\}| < |Re\{\mu\}|$. This can be done by finding the maximum approximation error caused, first, when calculating the periodic solution of the nonlinear system and its period and, second, when integrating the solution of the linear system (6). To find periodic solution of the system 1, one can approximate these solution with harmonic terms [31].Then the sum of the mentioned error, i.e. $\delta Re\{\mu\}$ must satisfy $|\delta Re\{\mu\}| < |Re\{\mu\}|$. The following inequality expresses the constraint obtained using this approach.

$$\begin{aligned} &\frac{1}{2\left|\mu_i\right|}\left|\boldsymbol{e}_i^T\left\{\delta\mathbb{J}_{\boldsymbol{f}}(\bar{\boldsymbol{x}}_M(0)) - 2\frac{\delta T_M}{T_M}\left[\mathbb{J}_{\boldsymbol{f}}(\bar{\boldsymbol{x}}_M(0)) - \mu_i^2 I\right]\right\}\boldsymbol{e}_i\right| \\ &+\frac{1}{T}\left|\log\left(1 + \frac{\boldsymbol{x}_N(t)^T\left\{\mathbb{J}_{\boldsymbol{f}}(\bar{\boldsymbol{x}}(T)) - 3\mu_N^2 I + (N+1)^2\omega^2 I\right\}\delta\boldsymbol{x}_N(t) - 2\mu_N^2\frac{\dot{\boldsymbol{x}}_N(T)^T\delta\dot{\boldsymbol{x}}_N(T)}{\dot{\boldsymbol{x}}_N(T)^T\dot{\boldsymbol{x}}_N(T)}\boldsymbol{x}_N(t)^T\boldsymbol{x}_N(t)}{\boldsymbol{x}_N(t)^T\left\{\mathbb{J}_{\boldsymbol{f}}(\bar{\boldsymbol{x}}(T)) - 5\mu_N^2 I + (N+1)^2\omega^2 I\right\}\boldsymbol{x}_N(t)}\right)\right| \\ &< \left|\mu_i\right|. \end{aligned} \tag{10}$$

Where $\boldsymbol{e}_i$ is the $i-$th column of the identity matrix, $\bar{\boldsymbol{x}}_k$ is the periodic solution of the system (5) approximated by k harmonic terms, $\mathbb{J}_{\boldsymbol{f}}$ is the Jacobian of the vector field $\boldsymbol{f}$, T_k represents the period of the solution $\bar{\boldsymbol{x}}_k$ (proof will be given in a forthcoming paper). This condition is used to determine how accurate the approximation of the periods, T_k, of the periodic orbits of the system (1) had to be in order to perform the stability analysis in Fig. 10. In contrast, Fig. 11 compares this approach with a more standard approach in which a fixed accuracy is used and the validity is not checked. The results in that case are highly inaccurate and hence difficult to interpret.

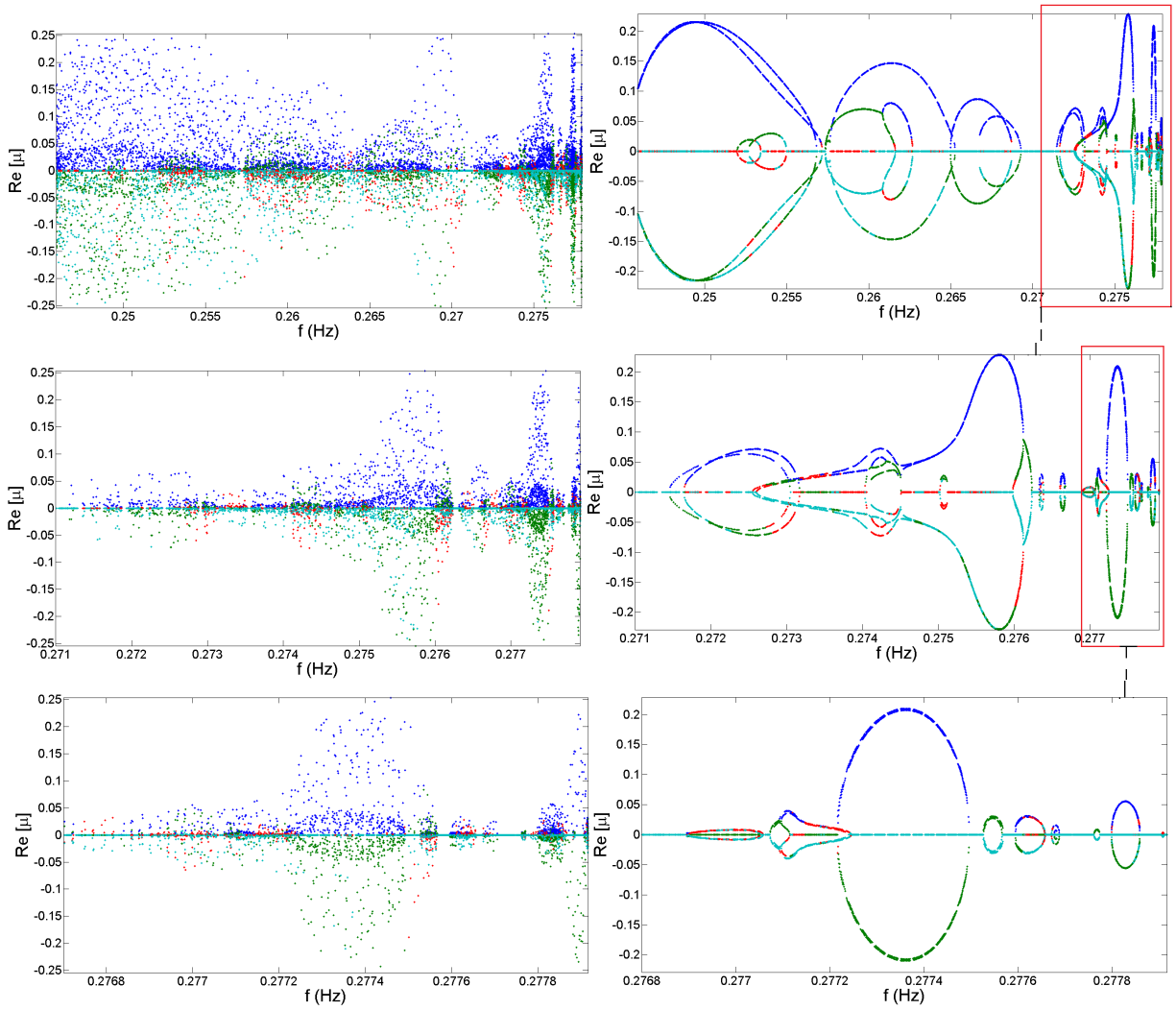

Figure 11: Floquet exponents calculated without satisfying the inequality (10) (left) and after satisfying (10) are shown for the ICM I-11,II-19 in Fig 10. Three regions, as shown in the right, have been magnified in both sets of valid and invalid computed Floquet exponents.

4.2 Stability of Periodic Orbits and Orientability of Their Local Invariant Manifolds

Orientability is a geometric property. In this sense, the orientability of an invariant manifold, such as those shown in Fig.6, can always be determined by finding its geometry. However, for more complicated geometries like the ones shown in Figs. 7-8, determining the orientability, although possible, is not trivial. For invariant

manifolds of dynamical systems, however, one can find the orientability of such manifolds by analyzing the behavior of the solutions of the system. For example, the geometries of the invariant manifolds of periodic orbits are shaped by the asymptotic behavior of the solutions that are initiated close to the orbits. The dynamics of such solutions, as mentioned earlier in this section, are governed by Eq. (6). Furthermore, since the Floquet exponents of the system in (6) dictate the asymptotic behavior of the mentioned solutions, they consequently determine the geometry of the invariant manifolds of their associated periodic orbit. In this regard, stability analysis (using Floquet exponents or multipliers) is essential for any quantitative approach to determine the orientability of the local invariant manifolds of periodic orbits. Explaining the relation between the stability of periodic orbits and the geometry of their local invariant manifold is the main focus of the (global) bifurcation theory.

Roughly speaking, bifurcation theory explains how fixed points of systems turn into (branches of) simple periodic orbits and how simple periodic orbits change into more complicated ones when they lose stability. The mechanisms that govern such transformations between different types of equilibrium are important, not only because they explain why and how such changes happen, but also because they can be used to predict when the changes happen and what they are. The latter feature of such mechanisms is the main tool for determining the orientability of invariant manifolds of periodic orbits. For example, when a simple periodic orbit, such as a solution that orbits on a circle on a cylinder, loses its stability, it may transform into a periodic orbit that moves on the surface of a twisted strip or a torus. What determines the geometry, where the resultant unstable periodic orbit travels on, is the mechanism, through which, the simple periodic orbit loses its stability. If the simple periodic orbit loses its stability through Andronov-Hopf bifurcation (torus bifurcation), then the resultant periodic orbit will travel on the surface of torus.

A thorough study of all possible types of bifurcation is beyond the scope of this paper. However, for the system 1, nine types of periodic orbits have been identified and are provided in Appendix A. Also two cases of bifurcations and their associated mechanisms of losing stability are presented in Appendix B.

5 Numerical Simulation of Jump Phenomena

Analysis of the free response of oscillatory systems is the foundation of many identification methods [38, 39, 40, 41]. In some, such as [42, 43], free responses of a slightly damped system have been used to identify the nonlinear modes of vibration of the underlying undamped system. Theses approaches use the decaying response of the system, initiated on a branch of nonlinear modes, to extract the frequency-energy dependence of the branch using time-frequency analysis tools such as a wavelet transform. This section reveals the sensitivity of such algorithms to the amount of damping and also the accuracy of the initial conditions. This is explicated by presenting examples of jump phenomena in the frequency of the response of the system for a set of different damping ratios and also accuracy of the initial conditions. This section also provides an explanation of these jumps using catastrophe theory, which describes the jump phenomena as a sudden change in the state of the system passing through local manifolds which are tangent to each other or manifolds with different orientability properties. In this sense, this study can help to extend the application of the aforementioned approaches, since, jumps are one of the primary factors preventing broader adoption of this type of identification.

5.1 Non-conservative System

The non-conservative system shown in Fig. 1 is considered herein with non-zero damping coefficients with the same underlying conservative system as the system in (1). The EOM of this system can be written as

$$\begin{bmatrix} \ddot{x}_1 \\ \ddot{x}_2 \end{bmatrix} = -\begin{bmatrix} 2 & -1 \\ -1 & 2 \end{bmatrix}\begin{bmatrix} x_1 \\ x_2 \end{bmatrix} - C\begin{bmatrix} \dot{x}_1 \\ \dot{x}_2 \end{bmatrix} - \begin{bmatrix} 0.5x_1^3 \\ 0 \end{bmatrix}. \tag{11}$$

or equivalently

$$\begin{bmatrix} \dot{x}_1 \\ \dot{x}_2 \\ \dot{y}_1 \\ \dot{y}_2 \end{bmatrix} = \begin{bmatrix} \mathbf{0}_{2\times 2} & \mathbf{I}_{2\times 2} \\ \begin{bmatrix} -2 & 1 \\ 1 & -2 \end{bmatrix} & -C \end{bmatrix}\begin{bmatrix} x_1 \\ x_2 \\ y_1 \\ y_2 \end{bmatrix} + \begin{bmatrix} 0 \\ 0 \\ -0.5x_1^3 \\ 0 \end{bmatrix} \tag{12}$$

where the damping matrix C is defined by

$$\begin{bmatrix} \mathbf{0}_{2\times2} & \mathbf{0}_{2\times2} \\ \mathbf{0}_{2\times2} & -C \end{bmatrix} = V^T \begin{bmatrix} \mathbf{0}_{2\times2} & \mathbf{0}_{2\times2} \\ \mathbf{0}_{2\times2} & \begin{bmatrix} 2\zeta_1\omega_1 & 0 \\ 0 & 2\zeta_2\omega_2 \end{bmatrix} \end{bmatrix} V \tag{13}$$

in which, $(i\omega, V)_i$ define the linearized modes of the conservative part of the system in (11). This way, one can readily find the damping matrix

$$\begin{aligned} C &= V^T \begin{bmatrix} 2\zeta_1\omega_{n1} & 0 \\ 0 & 2\zeta_2\omega_{n2} \end{bmatrix} V = 2 \begin{bmatrix} -\frac{\sqrt{2}}{2} & -\frac{\sqrt{2}}{2} \\ -\frac{\sqrt{2}}{2} & \frac{\sqrt{2}}{2} \end{bmatrix}^T \begin{bmatrix} \zeta_1 & 0 \\ 0 & \sqrt{3}\zeta_2 \end{bmatrix} \begin{bmatrix} -\frac{\sqrt{2}}{2} & -\frac{\sqrt{2}}{2} \\ -\frac{\sqrt{2}}{2} & \frac{\sqrt{2}}{2} \end{bmatrix} \\ &= \zeta_1 \begin{bmatrix} 1 & 1 \\ 1 & 1 \end{bmatrix} + \sqrt{3}\zeta_2 \begin{bmatrix} 1 & -1 \\ -1 & 1 \end{bmatrix}. \end{aligned} \tag{14}$$

that should be used to give two desired modal damping ratios in the system (11).

5.2 Cases of Jump Phenomena in the Free Response of the Non-conservative System

In this section, the system described in (11) is initiated at an initial condition that is on one of the periodic orbits on ICM I or ICM II, but with a small deviation δ. The time evolution of the solution is then calculated using the EOM defined in (11) for different values of ζ and δ. Then, the short time Fourier transform is used to obtain the spectrogram of the solution. The dominant frequency at each time instant is then extracted from the spectrogram. Figures 13-16 show the results of a few of these simulations in which jump phenomena are observed as the system looses energy along different invariant manifolds of the underlying conservative system. Two (out of many possible) scenarios are outlined next to explain these jumps as the interaction between invariant manifolds of the system.

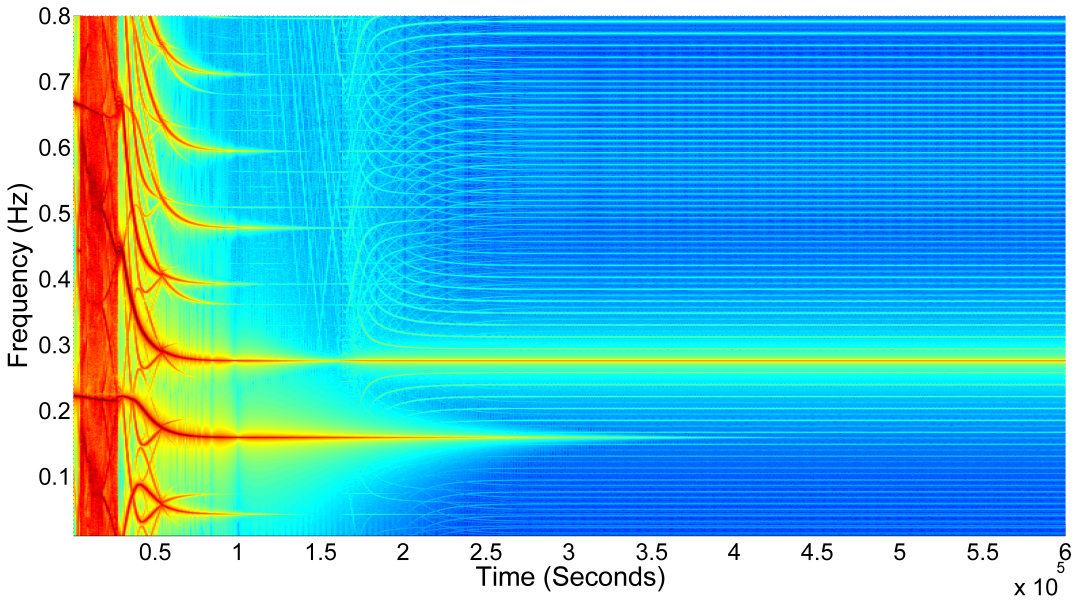

Figure 12: Time-frequency history of the solution of the system, initiated on the ICM II, is calculated using short-window Fourier transform.

In order to explain the jumps in the dominant frequency of solution of the system, for example in the time-frequency plot shown in Fig.12, some background could be beneficial. This is provided next. Moving along an invariant manifold of the system, in this case the local center manifold or local ICM, the solution of of the system may change its path from one manifold to another manifold that comes to contact with it. In this scenario, in order for such a change to happen, two ingredients are required. First, the two mentioned manifolds should be tangent to each other at the state where the solution changes its course from one to another. This tangency or non-transversality can be captured by the resonance condition or equivalently in the transversality condition. At the resonance condition, the Jacobian of the linearized system around the equilibrium becomes singular, indicating that its manifold may have more than one tangent plane at that equilibrium. The non-transversality condition described in Eq. (17) expresses the same concept in terms of (real part of) Floquet exponents and the change in the stability of the equilibrium. Second, the solution of the system needs to be perturbed (or be in a perturbed state) while passing through the neighborhood of the non-transversal intersection. In this regard, the initial perturbation δ is imposed to the solution of the system on the local ICMs. Note that when the manifold (NNM branch) is stable, the deviation δ will gradually decay due to damping until it is no longer strong enough to cause a jump in thepath of the solution.

Jump phenomena may also occur when the solution of the system changes its pathbecause of the orientability properties of the manifolds on its path. The manifold described by one of the NNM branches is typically a curvilinear plane or a twisted strip. It may be intersected by a variety of other manifolds. For example, suppose that the second manifold is a closed orientable manifold such as a torus. In this case, the solution of the system cannot lose energy by orbiting outside of the torus and needs to move to the inside. That is not possible because torus defines an orientable manifold. In such cases, a jump to the next open manifold is likely to happen. On the other hand, a twisted Mobius stripes and twisted strips are both open (nonorientable and orientable) manifolds where the solution of the system can lose energy while orbiting on one side of the manifold without having to cross it, and so, the response of the system is likely to stay on this type of manifold and not exhibit a jump.

Figure 13, shows an example where the solution was initiated on the ICM II with $\delta = 0.05\%$ deviation in its initial condition. The damping ratio was set to $\zeta_{1,2} = 1e-7$. Each neighborhood of the points marked with circles (denoted by letters A to F) houses two consecutive jumps which will be explained next. Starting (almost) on ICM II, the solution of the system begins losing energy on one side of ICM II (an orientable Twisted strip) until it hits point A. Two consecutive jumps, one because of non-transversality and another because of an orientable torus happens in the neighborhood A. First, the solution jumps from ICM II to ICM I-5,II-15 because of non-transversal intersection of the ICM II and the ICM I-5,II-15 manifolds become tangent (15:1 resonance). However, this jump is not evident in the dominant frequency shown in Fig 13, because, the scaling function described in (3) is used to scale the dominant frequency. In the absence of this scaling function, the dominant frequency would be seen to jump to 1/15th of the ICM II frequency. Then, since the manifold ICM I-5,II-15, at the neighborhood of A is a torus, the solution jumps again to ICM I in the neighborhood B where ICM I is locally a orientable twisted Mobius strip. The solution continues to lose energy until it reaches the end of the neighborhood B where the local ICM I is tangent to ICM II (3:1 resonance-the local ICM of this point is visualized in Fig (8)- Middle-Left). At this point, the solution jumps back on the ICM II and continues to lose energy on one side of its orientable twisted strip until it enters in the neighborhood C. Same set of jumps as in the neighborhood A happens in neighborhood C causing the solution to jump down on the ICM I which is locally an orientable twisted strip in the neighborhood D. Another sets of two consecutive jumps similar to neighborhoods A and C, send the solution back up to the ICM II (neighborhood E) and then down to ICM I (neighborhood F). However, at this point, the deviation δ has decayed to a level that is not enough to cause any other jumps at the upcoming points prone to jump at its path on ICM I.

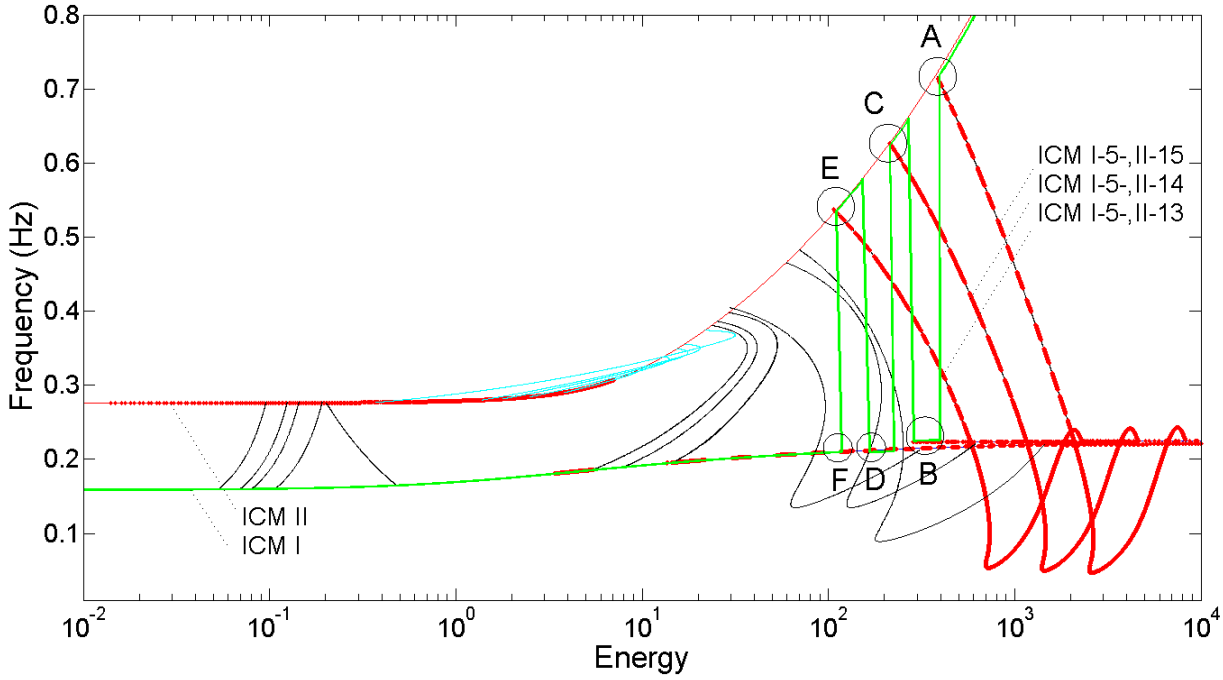

Figure 13: Dominant frequency of the decaying solution of the system is overlaid on top of ones from identified ICMs of the underlying conservative system. Unstable periodic orbits are shown in red dots for five of the ICMs, i.e. ICM I, ICM II, ICM I-5,II13,ICM I-5,II14 and ICM I-5,II15. Jumps occur at six neighborhood labeled A to F.

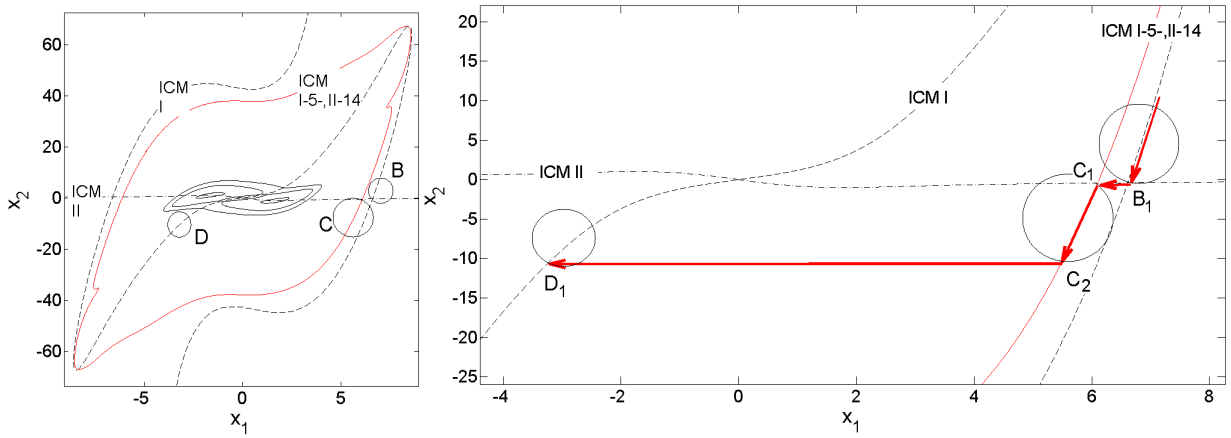

Figure 14: Left: Poincare map sowing the ICMs I, II and I-5,II-14. Right: Magnified view showing the solution of the system at the neighborhood B and C highlighted by red arrows.

These jumps are examined in more detail in Fig. 14, which shows a cross section of a Poincare map of the system (defined in Section. 2) that shows several of the ICMs of the system in the neighborhoods B and C that were marked in Fig. 13. Moving along the the ICM I, the solution reaches the non-transversal intersection between the ICM I and ICM II at the point B_1 in the neighborhood B. At this point the deviation δ causes the solution to jump from ICM I to ICM II and continue on it until it reaches the point C_1 in the neighborhood C. At this point the ICM II and ICM I-5-II-14 intersect non-transversaly and the solution jumps onto the ICM I-5-II-14 and it continues on ICM II until point C_2. The point C_2 represents a periodic

solution that orbits on the surface of a torus (its local ICM) . The periodic orbit at C_2 is the product of the periodic orbit at C_1 after losing stability through torus bifurcation. At this point, since the solution cannot lose energy by orbiting outside of a torus and also cannot move through it, since the torus is orientable, it jumps again onto the ICM I in the neighborhood D.

In another case, shown in Fig. 15, the solution, which was initiated on ICM I, reveals a similar set of jumps at the neighborhood B, C, and D and finally rest at ICM II.

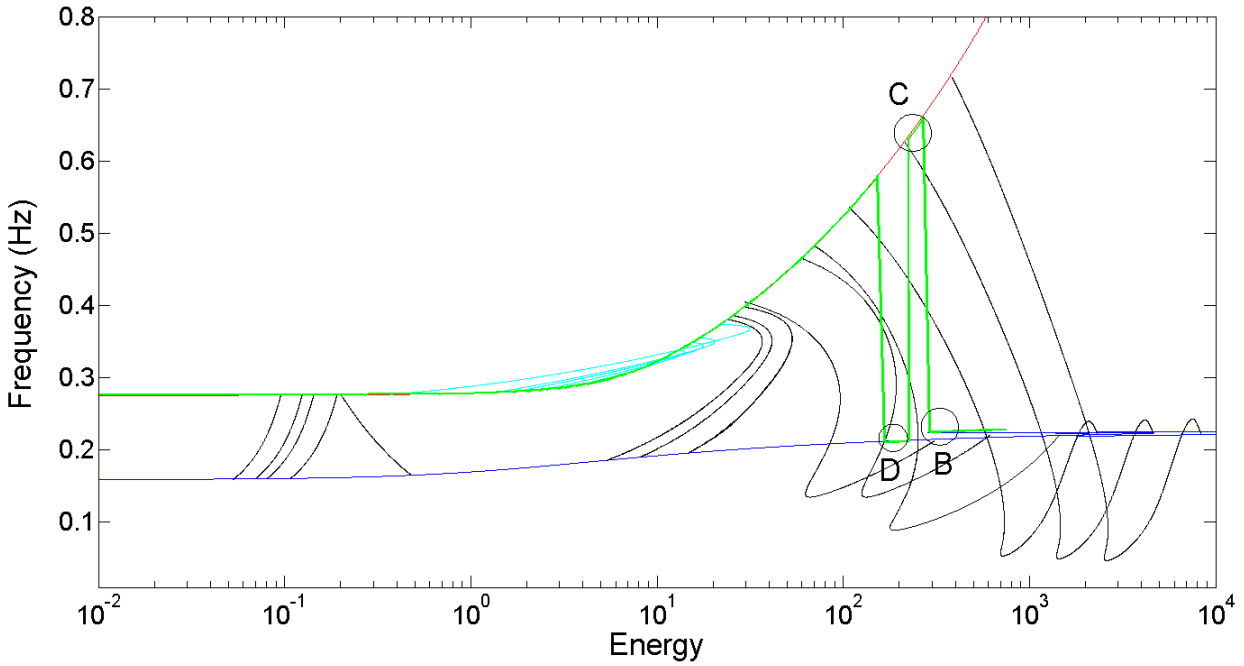

Figure 15: Dominant frequency of the decaying solution of the system initial (almost) on the ICM I with $\delta = 0.05\%$ and $\zeta = 1e-6$. At thre neighborhood B, C, and D the divination of the solution from the periodic orbits of the underlying conservative system forces the solution to move form one ICM to another one at their non-transversal intersections causing the frequency of the solution to jump. It's worth noting that although the solution was initiated on the ICM I, it reaches the origin through losing energy on the ICM II.

As explained earlier, damping also causes the deviation to decay as the solution advances. This effect is evident at the neighborhood F where the deviation has decayed to such an extent that it is not enough to cause another jump despite the existing potential for another set of jumps at its next encounters with non-transversal intersections. This effect can be further examined by recomputing the response with a damping ratio $\zeta_{1,2} = 1e-6$, that is ten times larger than what was used in Fig. 13. To illustrate this effect, the dominant frequency of the solution of the system (for the same set of initial conditions and deviation) are obtained for damping ratios $\zeta_1 = \zeta_2 = \{5e-7, 1e-6, 12e-6\}$. As shown in Fig. 16, increasing the damping ratio will cause a the initial deviation to decay more quickly so that it falls below the level at which it is sufficient to cause a jump at a non-transversal intersection. At $\zeta = 12e-6$, the initial deviation is damped enough before the solution reaches the first non-transversal intersection. It is worth mentioning that decreasing the initial deviation has the exact same effect as increasing the damping ration on the behavior of the solution at non-transversal intersections on its path.

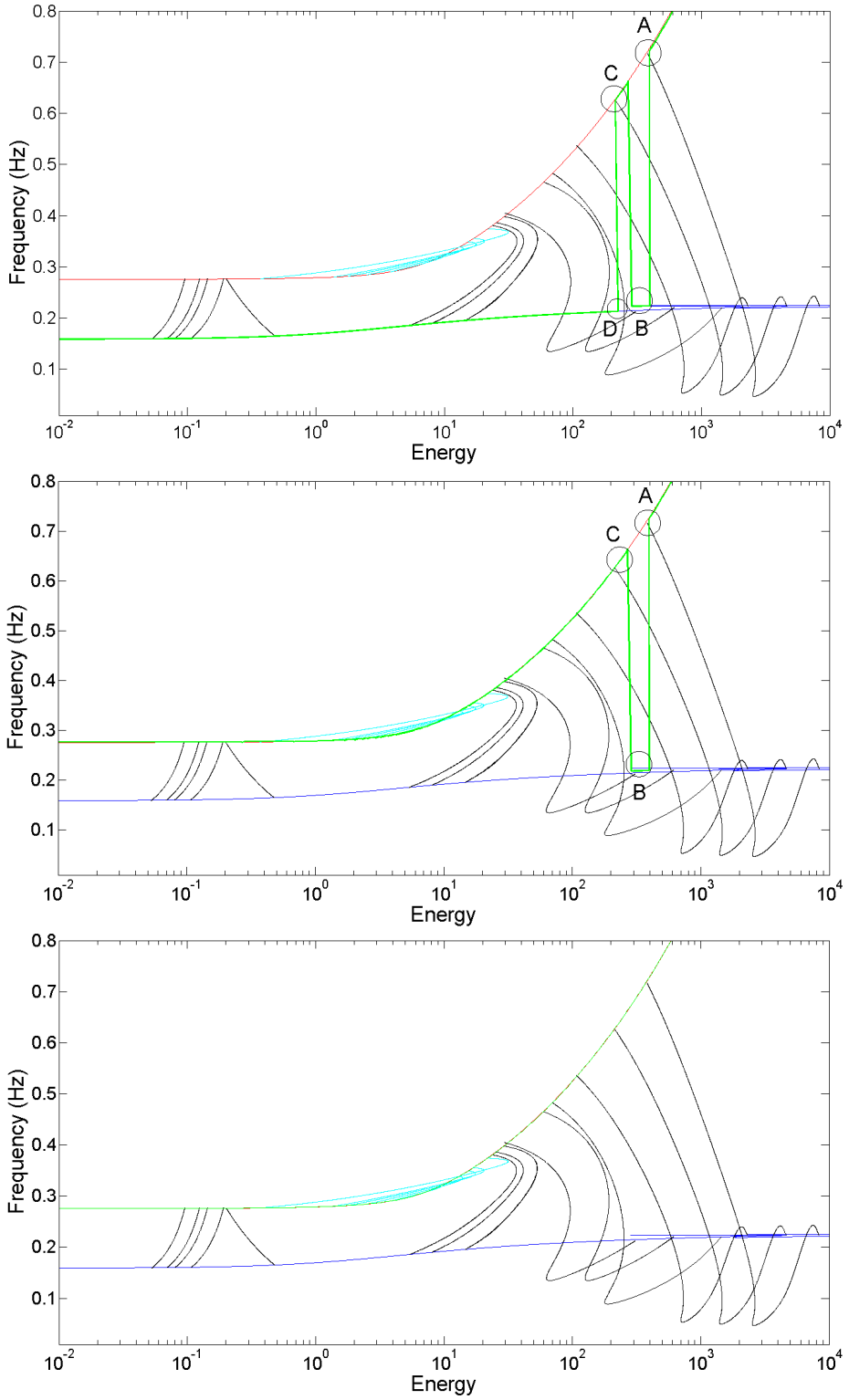

Figure 16: Dominant frequency of the solution of the damped system, shown with a solid green line, obtained for damping ratios $\zeta = \{5e-7,\ 1e-6,\ 12e-6\}$. Increasing the damping ratio, while the initial deviation was held fixed, has caused the initial deviation to decay quickly to below the level at which it is large enough to perturb the solution at its first encounter with the non-transversal intersection at neighborhood A and at all subsequent intersections. It is also interesting to note that the response continues to decay along the ICM II even though many of the periodic orbits are unstable for energies below 10^1.

6 Conclusion

This paper has showed that catastrophe theory and bifurcation theory can be used to understand abrupt discontinuities in the response of a dynamical system. While this is a concept that has attracted scientists and engineers for centuries and the bifurcation and catastrophe theory that have been employed are not new, this work has sought to connect these concepts to modes of vibration and (internal) resonance. In this regard, this paper presented a brief introduction of an extended definition of modes of vibration, i.e. nonlinear modes, through the concept of ICM. Three different representation of such modes are provided for a two DOF nonlinear conservative system. One key tool that is needed in this type of analysis is a means of calculating the stability of periodic orbits. Although the concept is well established, this is incredibly challenging for a nonlinear system based on numerical ICMs or NNMs. Here a new criteria was presented that makes this possible

This study discussed the effect of nonlinear modes on the solutions of nonlinear systems through geometric concepts such as the loci of nonlinear modes (ICMs) and their orientability. These concepts are explicated by few examples of orientable and nonorientable ICMs of the nonlinear modes of the case study. An explanation is provided at two qualitative and quantitative levels that relates the bifurcation theory, catastrophe theory and the geometric properties of the ICMs of nonlinear systems. Furthermore, a slightly damped adaptation of the cases study is presented. Decaying response of the system is studied using time-frequency analysis. Results reveal multiple cases of jump phenomena which were explained through catastrophes and bifurcations caused by non-transversal (tangential) intersection of ICMs.

The findings presented here can be used in several ways. As mentioned previously, they explain why it is sometimes difficult to force a system to decay along one of its NNMs as is required in the identification method in [43]. This may lead to a better understanding of what classes of systems are most suitable for that identification method and how to increase the probability of success. One other application, is to utilize to find the ICMs (branches of nonlinear modes) that are not continuations of linear modes. Regions that exhibits jump phenomena can be searched for new nonlinear modes by initiating continuation algorithms at different directions.

Appendix A: Orientability of Periodic Solutions

This section explains a quantitative approach that can determine the orientability property of local invariant manifolds using the Floquet multipliers and exponents of the corresponding periodic orbit about which the manifold was created. In this approach , first, periodic orbits are categorized based on their Floquet exponents as shown in Table 1. Then , the orientability of both the local stable and unstable manifolds, if they exist, are determined using Floquet multipliers. This orientability property is the key to understanding whether a periodic orbit can be reached by the system from a particular region in the state space, and hence whether the system is likely to jump or remain on a particular solution branch. For example, in the damped system studied herein, since the system is losing energy, it will always approach any periodic orbit, on its path, from its local stable manifold. Therefore, if the stable manifold of a periodic orbit is orientable, the periodic orbit in question will not affect the the path of the solution of the system. In this study, these periodic orbits are referred to as isolated periodic orbits. Next, the orientability of local center manifold is determined using Floquet multipliers. However, local center manifold do not always exist. In such cases, one can assign the orientability of the local ICM to the periodic orbit. That is because, the orientability of the local center manifold and the local ICM should agree at all times since ICMs are the loci of all periodic orbits of the system. In other words, in such cases , periodic orbits adopt the orientability of the center manifolds of periodic orbits in their neighborhood on the local ICM.

The basis in identifying the orientability property of local stable and unstable manifolds of periodic orbits is the fact that Floquet multipliers of a periodic orbit are the same as eigenvalues of its Poincare map [37, 44, 45]. In [46, 47, 48] it was shown that a local manifold is orientable if all of the eigenvalues of its Poincare map are real and positive. This was done using the fact that the Poincare map is an orientation preserving map[2].

[2]Poincare map is a rotation matrix with unity determinant.

Periodic Orbit Type	Floquet Exponent	Stable Manifold / Unstable Manifold	Center Manifold/ICM
1. Center 1 (Center-Center)	$\mu_1 = i\psi_1$ $\mu_2 = -i\psi_1$ $\mu_3 = i\psi_2$ $\mu_4 = -i\psi_2$	$\emptyset$ $\emptyset$	4D Orientable Surface (curvilinear planes)
2. Sink 1 (Sink-Sink)	$\mu_1 = -\lambda_1 + i\psi_1$ $\mu_2 = -\lambda_1 - i\psi_1$ $\mu_3 = -\lambda_2 + i\psi_2$ $\mu_4 = -\lambda_2 - i\psi_2$	4D $\rho_i\|_{i=3}^4 = \begin{cases} \in \mathbb{R}^+ & \text{Onorientable} \\ otherwise & \text{Nonorientable} \end{cases}$ Stable	$\emptyset$, 2D $p+q = \begin{cases} 2k+1 & \text{Nonorientable} \\ 2k & \text{Orientable} \end{cases}$ surface
3. Sink 2 (Sink-Center)	$\mu_1 = i\psi_1$ $\mu_2 = -i\psi_1$ $\mu_3 = -\lambda_2 + i\psi_2$ $\mu_4 = -\lambda_2 - i\psi_2$	2D $\rho_i\|_{i=3}^4 = \begin{cases} \in \mathbb{R}^+ & \text{Onorientable} \\ otherwise & \text{Nonorientable} \end{cases}$ Stable	2D Orientable Torus
4. Source 1 (Source-Source)	$\mu_1 = \lambda_1 + i\psi_1$ $\mu_2 = \lambda_1 - i\psi_1$ $\mu_3 = \lambda_2 + i\psi_2$ $\mu_4 = \lambda_2 - i\psi_2$	4D $\rho_i\|_{i=1}^4 = \begin{cases} \in \mathbb{R}^+ & \text{Onorientable} \\ otherwise & \text{Nonorientable} \end{cases}$ Unstable	$\emptyset$, 2D Orientable Torus
5. Source 1 (Source-Center)	$\mu_1 = i\psi_1$ $\mu_2 = -i\psi_1$ $\mu_3 = \lambda_2 + i\psi_2$ $\mu_4 = \lambda_2 - i\psi_2$	2D $\rho_i\|_{i=3}^4 = \begin{cases} \in \mathbb{R}^+ & \text{Onorientable} \\ otherwise & \text{Nonorientable} \end{cases}$ Unstable	2D Orientable Torus
6. Saddle 1 (Saddle-Saddle)	$\mu_1 = \lambda_1$ $\mu_2 = -\lambda_1$ $\mu_3 = \lambda_2$ $\mu_4 = -\lambda_2$	2D Orientable Stable 2D Orientable Unstable	$\emptyset$, 2D $p+q = \begin{cases} 2k+1 & \text{Nonorientable} \\ 2k & \text{Orientable} \end{cases}$ surface
7. Saddle 2 (Saddle-Center)	$\mu_1 = \lambda_1$ $\mu_2 = -\lambda_1$ $\mu_3 = i\psi_1$ $\mu_4 = -i\psi_1$	1D Stable Curve 1D Unstable Curve	2D Orientable Torus
8. Saddle 3 (Source-Sink)	$\mu_1 = -\lambda_1 + i\psi_1$ $\mu_2 = -\lambda_1 - i\psi_1$ $\mu_3 = \lambda_2 + i\psi_2$ $\mu_4 = \lambda_2 - i\psi_2$	2D $\rho_i\|_{i=}^2 = \begin{cases} \in \mathbb{R}^+ & \text{Onorientable} \\ otherwise & \text{Nonorientable} \end{cases}$ Stable 2D $\rho_i\|_{i=3}^4 = \begin{cases} \in \mathbb{R}^+ & \text{Onorientable} \\ otherwise & \text{Nonorientable} \end{cases}$ Unstable	$\emptyset$, 2D Orientable Torus
9. Saddle 4 (Source-Sink)	$\mu_1 = -\lambda_1 + i\psi_1$ $\mu_2 = -\lambda_1 - i\psi_1$ $\mu_3 = \lambda_1 + i\psi_1$ $\mu_4 = \lambda_1 - i\psi_1$	2D $\rho_1 = \begin{cases} \in \mathbb{R}^+ & \text{Onorientable} \\ otherwise & \text{Nonorientable} \end{cases}$ Stable 2D $\rho_1 = \begin{cases} \in \mathbb{R}^+ & \text{Onorientable} \\ otherwise & \text{Nonorientable} \end{cases}$ Unstable	$\emptyset$, 2D Orientable Torus

Table 1: Nine types of periodic orbits are identified for the system (1) based on their Floquet multiplier and exponents. Floquet multipliers and exponents are denoted by ρ and μ respectively.

The orientability of a local center manifold is based on the type of bifurcation that has generated it. In this study, the system exhibits, mostly, three types of bifurcations, namely, Hopf-Hopf bifurcations, Period-Doubling bifurcations and Andronov-Hopf (or Torus) bifurcations. One can determine which type of bifurcation one has based on the Floquet multipliers of the periodic orbit, as will be discussed in the next section. In this regard, the local center manifold of a periodic orbit is:

- an orientable curvilinear plane if it is originated from a Hopf-Hofp bifurcation,
- a twisted strip with k half-twists (orientable for even k and nonorientable for odd k) if it is originated from a Period-Doubling bifurcation, or
- an orientable torus if it is originated from an Andronov-Hopf (torus) bifurcation.

In cases where the local center manifolds do not exist, such as cases of periodic orbits with Period-Doubling bifurcations, the local ICMs can be used to determine the orientability property of the periodic orbits. In this regard, since, all coordinates of a periodic solutions are also periodic, one can assume an analytical representation of the ICMs [31] of the system 1 as

$$\begin{aligned} x_1 &= \Sigma A_m^{(1)} \cos m\phi_1 = \cos\phi_1 \left(A_1^{(1)}(T) + \Sigma_{m=2} \left[A_m^{(1)} \cos m\phi_1 \right] \right) \\ H_{x_1} &= \Sigma A_m^{(1)} \sin m\phi = \sin\phi_1 \left(A_1^{(1)} + \Sigma_{m=2} \left[A_m^{(1)} \sin m\phi_1 \right] \right) \\ x_2 &= \Sigma A_m^{(2)} \cos m\phi_2 = \cos\phi_2 \left(A_1^{(2)} + \Sigma_{m=2} \left[A_m^{(2)} \cos m\phi_2 \right] \right) \end{aligned} \tag{15}$$

where ϕ_i's, in general, are

$$\begin{aligned}\phi_1 &= q\phi_0 \\ \phi_2 &= p\phi_0\end{aligned} \tag{16}$$

and , $\phi_0 = \frac{2\pi}{T}t$ and T represents the period of the periodic orbits. Equation (15), in general[3], defines a twisted strip with $p+q$ half-twists (see ruled surfaces in [49, 50]). In this sense, following the discussed in Section 3, if $p+q$ is odd, then (15) defines a nonorientable surface. On the other hand, the surface is orientable if $p+q$ is even.

To this end, nine types of periodic orbits are identified and the orientability of their local invariant manifolds (including the local ICM) are summarized in Table 1. It is importance to mention that Table 1 is obtained applies only to a 2 DOF conservative oscillatory system and is far from providing a complete list for a general dynamical system in $\mathbb{R}^4$.

Appendix B: Mechanisms of Losing Stability (Cases of Local and Global Bifurcations)

Section 4.1 discussed how the stability of a periodic orbit manifests itself through Floquet multipliers (or exponents). Section 4.2 presented the relationship between the Floquet multipliers (or exponents) and the orientability of the local invariant manifolds of the periodic orbits. This section, explains some of the mentioned relations based on mechanisms through which fixed points or periodic orbits lose stability and as a result new periodic orbits come to exist. These mechanisms describe the change in the structure of the geometry of the periodic orbits and their local invariant manifolds as a function of the change in their period. In this regard two mechanisms explaining two types of bifurcations, with an eminent role in the system 1, are presented. Note that the system in 1 exhibits a very rich set of different types of bifurcations, including some special cases. However, the study of all such cases of bifurcations is beyond the scope of this paper. For more details on different types of bifurcation, specially in $\mathbb{R}^4$, readers are referred to [37, 51, 45, 35].

6.1 Bifurcations of Periodic Orbits from a Fixed Point

Hopf-Hopf Bifurcation- An equilibrium point is referred to as a Hopf-Hopf point (or double Hofp point) if, at the mentioned point; first, the system has only two pairs of purely imaginary eigenvalues, i.e. $\pm i\omega_1, \pm i\omega_2$ and, second, if the change in the imaginary part of the Floquet exponents with respect to the period is zero, or specifically, the transversality (generosity) condition (see [37, 51, 35])

$$\frac{d}{dT}\mu_i = 0 \tag{17}$$

is satisfied. This is a broad definition that also includes unusual Hopf points. In a four dimensional system, at a Hopf-Hopf point many cases of bifurcation can occur which are described in [51]. In the case of the system 1, bifurcation of double Hopf points is the birthplace of four (half) branches of periodic orbits on two dimensional invariant linear (and later curvilinear) planes. These branches of periodic orbits include linear modes of vibration and their nonlinear continuation. In this sense, one can state that the Hopf-Hopf bifurcation of the fixed point of the system (1) is the birthplace of the modes of vibration in that neighborhood.

[3] In some special cases, such as where $\phi_2 = \frac{(2k+1)\pi}{2} - \frac{l}{2}\phi_1$, $k, l \in \mathbb{N}$, Eq. (15) generates Tori.

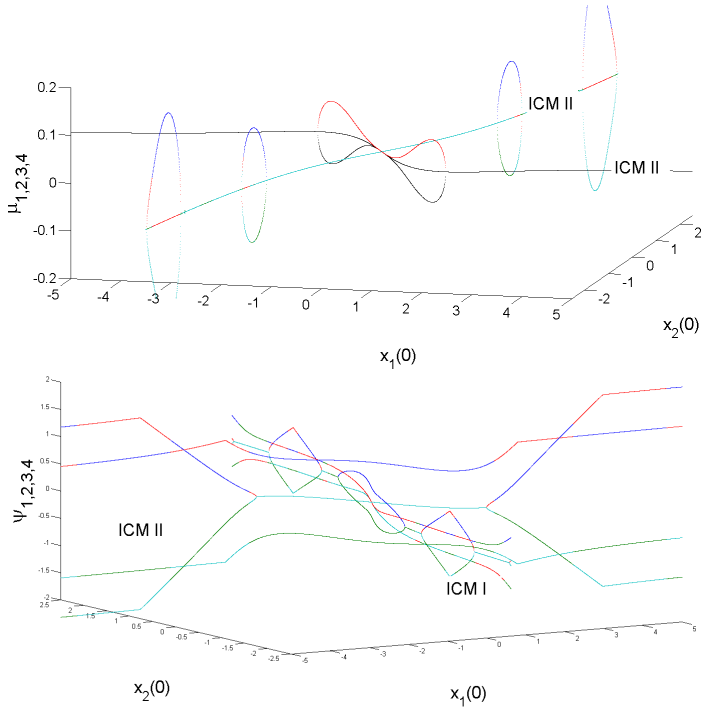

Figure 17: Top: Real parts of Floquet exponents calculated for ICM I and ICM II and shown on the cross-section of the Poincare map described in Section 2. The period T is defined as an descending variable along theses branches as they move away from the fixed point at the origin. The transversality (generosity) condition, i.e. $\frac{d\mu_i}{dT} = 0$, is satisfied at the fixed point of the system (1) at the origin. Therefore, the fixed point at the origin is double Hopf point for the system (1). Bottom: Imaginary parts of Floquet exponents calculated for ICM I and ICM II.

6.2 Bifurcations of Periodic Orbits from a Periodic Orbit

Neimark-Sacker Bifurcation- Neimark-Sacker (Torus) bifurcation[4] is characterized by a pair of complex conjugate multipliers crossing the unit circle at

$$\rho = e^{\pm i\phi},\ \phi \neq 0, \pi. \tag{18}$$

The bifurcation into a torus only happens in three or higher dimensional systems. In this case, a periodic orbit, that has lost its stability, spirals around a torus. This is schematically shown for a 3 dimensional case in Fig 18. Moreover, as shown in Fig. 18, in case of a torus bifurcation, the fixed point of Poincare map becomes unstable and generates limit cycles.

[4]It is sometimes called Hopf bifurcation of periodic orbits, secondary Hopf bifurcation or generalized Hopf bifurcation.

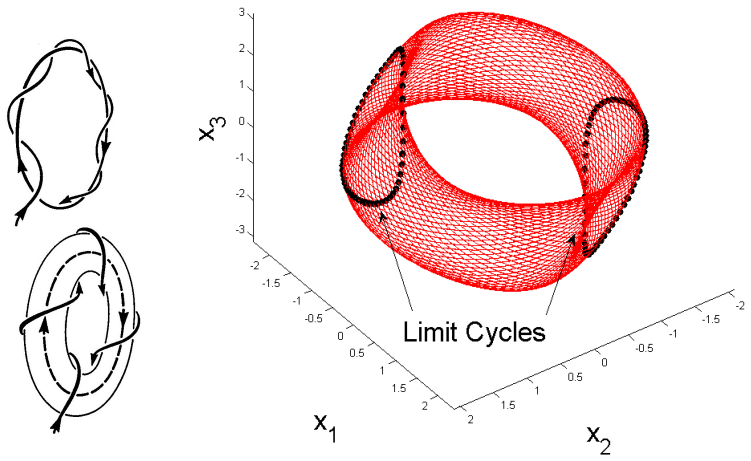

Figure 18: Left: A schematic illustration of torus bifurcation. A stable periodic orbit becomes unstable surrounded by a stable 2D torus. Right: Poincare map (shown with black dots) of a periodic orbit (shown in solid red) initiated at (0.9061 -1.6894, 0, 0). Appearance of limit cycles in the Poincare map reveals a case of torus bifurcation.

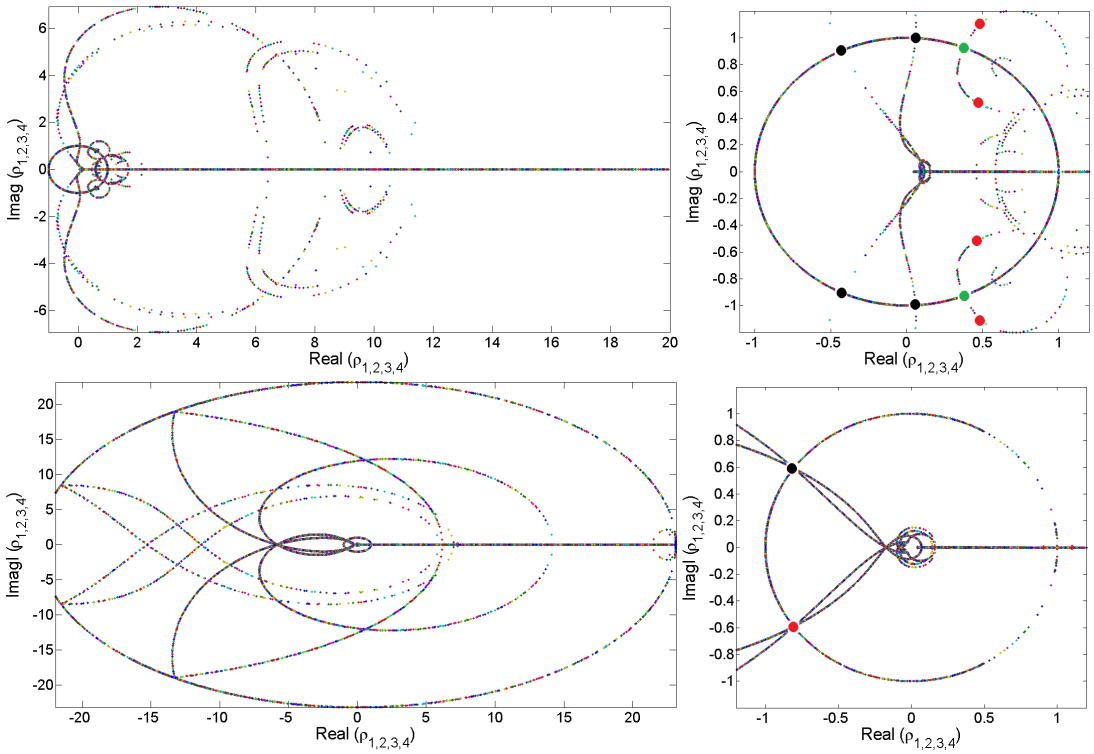

Figure 19: Left: Real part of Floquet multipliers calculated for ICM I-5,II-9 (Top) and ICM II-56 (Bottom). Right: Floquet multipliers of ICM I-5,II-9 (Top) and ICM II-56 (Bottom) in the neighborhood of the unit circle.

Numerous cases of torus bifurcations occur in the system (1). This can be observed in Figure 19 which shows the Floquet multipliers of two branches of periodic orbits. For example, in ICM I-5,II-9, the type-4

periodic orbits (in Table 1) bifurcate from the periodic orbit with multipliers shown in solid black circles through torus bifurcation . Both pairs of multipliers move outside the unit circle. The type-8 periodic orbits shown in red solid circles are the products of torus bifurcation of the periodic orbit with multipliers shown in solid green circles. In addition, in ICM II-56, the type-9 periodic orbits are created through torus bifurcation of the periodic orbit with multipliers shown in solid black circles. A pair of multipliers move inside the unit circle while the other one move inside.

References

[1] H. Yasui, H. Marukawa, Y. Momomura, and T. Ohkuma. Analytical study on wind-induced vibration of power transmission towers. *Journal of Wind Engineering and Industrial Aerodynamics*, 83(1):431–441, 1999.

[2] J. Shaw, S.W. Shaw, and A.G. Haddow. On the response of the non-linear vibration absorber. *International Journal of Non-Linear Mechanics*, 24(4):281–293, 1989.

[3] S.S. Oueini, C.M. Chin, and A.H. Nayfeh. Dynamics of a cubic nonlinear vibration absorber. *Nonlinear dynamics*, 20(3):283–295, 1999.

[4] X. Jiang, D.M. McFarland, L.A. Bergman, and A.F. Vakakis. Steady state passive nonlinear energy pumping in coupled oscillators: theoretical and experimental results. *Nonlinear Dynamics*, 33(1):87–102, 2003.

[5] A. Murata, Y. Kume, and F. Hashimoto. Application of catastrophe theory to forced vibration of a diaphragm air spring. *Journal of sound and vibration*, 112(1):31–44, 1987.

[6] K. SHIMOZAWA and T. TOHTAKE. An air spring model with non-linear damping for vertical motion. *Quarterly Report of RTRI*, 49(4):209–214, 2008.

[7] Y. Huang and S. Iwamoto. Analysis of a possible reason for oscillation phenomena in a diesel-generator set through catastrophe theory. *Energy Conversion, IEEE Transactions on*, 10(4):700–705, 1995.

[8] DJ Ewins. A study of resonance coincidence in bladed discs. *Journal of Mechanical Engineering Science*, 12(5):305–312, 1970.

[9] DJ Ewins. Vibration characteristics of bladed disc assemblies. *Journal of Mechanical Engineering Science*, 15(3):165–186, 1973.

[10] D. Afolabi and B. Alabi. Catastrophe theory, curve veering and the vibration of bladed discs. *Proceedings of the Institution of Mechanical Engineers, Part C: Journal of Mechanical Engineering Science*, 206(2): 143–144, 1992.

[11] W.M. Adams. *Analytic prediction of airplane equilibrium spin characteristics*, volume 6926. National Aeronautics and Space Administration, 1972.

[12] T. Hacker. A discussion of the roll-coupling problem. *Progress in aerospace sciences*, 15:151–180, 1974.

[13] AA Schy and ME Hannah. Prediction of jump phenomena in roll-coupled maneuvers of airplanes. *J. Aircraft*, 14(4):375–382, 1977.

[14] PJ Holmes and DA Rand. The bifurcations of duffing's equation: An application of catastrophe theory. *Journal of Sound and Vibration*, 44(2):237–253, 1976.

[15] T. Fang and EH Dowell. Numerical simulations of jump phenomena in stable duffing systems. *International journal of non-linear mechanics*, 22(3):267–274, 1987.

[16] Y. Ueda. Randomly transitional phenomena in the system governed by duffing's equation. *Journal of Statistical Physics*, 20(2):181–196, 1979.

[17] MJ Brennan, I. Kovacic, A. Carrella, and TP Waters. On the jump-up and jump-down frequencies of the duffing oscillator. *Journal of Sound and Vibration*, 318(4):1250–1261, 2008.

[18] R. Thom. *Stabilité structurelle et morphogénèse*. WA Benjamin Reading, Massachusetts, 1972.

[19] EC Zeeman. The geometry of catastrophe. *Times Literary Supplement*, 10:1556–7, 1971.

[20] H. A. Ardeh and D. Negrut. Instantaneous center manifolds: An approach for approximating the dynamics of nonlinear systems. *ASME Journal of Computational and Nonlinear Dynamics*, Submitted, 2011.

[21] R.M. Rosenberg and C.P. Atkinson. On the natural modes and their stability in nonlinear two-degree-of-freedom systems. *Journal of Applied Mechanics*, 26:377–385, 1959.

[22] R.M. Rosenberg. Normal modes of nonlinear dual-modes systems. *Institute of Engineering Research, University of California*, 1959.

[23] R.M. Rosenberg and American Society of Mechanical Engineers. The normal modes of nonlinear n-degree-of-freedom systems. ASME, 1961.

[24] R.M. Rosenberg. On normal vibrations of a general class of nonlinear dual-mode systems. *Journal of Applied Mechanics*, 29:7–14, 1962.

[25] R.M. Rosenberg. On nonlinear vibrations of systems with many degrees of freedom. *Advances in Applied Mechanics*, 9(155-242):6–1, 1966.

[26] S.W. Shaw and C. Pierre. Non-linear normal modes and invariant manifolds. *Journal of Sound and Vibration*, 150(1):170–173, 1991.

[27] S.W. Shaw and C. Pierre. Normal modes for non-linear vibratory systems. *Journal of Sound and Vibration*, 164(1):85–124, 1993. ISSN 0022-460X.

[28] S.W. Shaw and C. Pierre. Normal modes of vibration for non-linear continuous systems. *Journal of sound and vibration*, 169(3):319–347, 1994.

[29] G. Kerschen, M. Peeters, J.C. Golinval, and AF Vakakis. Nonlinear normal modes, Part I: A useful framework for the structural dynamicist. *Mechanical Systems and Signal Processing*, 23(1):170–194, 2009. ISSN 0888-3270.

[30] M. Peeters, R. Viguié, G. Sérandour, G. Kerschen, and J.C. Golinval. Nonlinear normal modes, part ii: Toward a practical computation using numerical continuation techniques. *Mechanical systems and signal processing*, 23(1):195–216, 2009.

[31] H. A. Ardeh and M. S. Allen. instantaneous center manifolds and nonlinear modes of vibrations. In *Proceedings of the ASME 2012 International Design Engineering Technical Conferences & Computers and Information in Engineering Conference*. ASME, 2012.

[32] T. Poston and I. Stewart. *Catastrophe theory and its applications*, volume 2. Dover Publications, 1996.

[33] I. Stewart. The seven elementary catastrophes. *New Scientist*, 68(976):447–454, 1975.

[34] I. Stewart. Elementary catastrophe theory. *Circuits and Systems, IEEE Transactions on*, 30(8):578–586, 1983.

[35] V.I. Arnol'd. Lectures on bifurcations in versal families. *Russian Mathematical Surveys*, 27(5):54, 2007.

[36] M.W. Hirsch, C.C. Pugh, and M. Shub. *Invariant manifolds*. Springer, 1977. ISBN 3540081488.

[37] I.U.A. Kuznetsov. *Elements of applied bifurcation theory*, volume 112. Springer Verlag, 1998.

[38] SF Masri, RK Miller, AF Saud, and TK Caughey. Identification of nonlinear vibrating structures: Part i–formulation. *Journal of Applied Mechanics*, 109(4):918–922, 1987.

[39] SF Masri, RK Miller, AF Saud, and TK Caughey. Identification of nonlinear vibrating structures: Part ii–applications. *Journal of Applied Mechanics*, 109(4):923–929, 1987.

[40] G.B. Giannakis and E. Serpedin. A bibliography on nonlinear system identification. *Signal Processing*, 81(3):533–580, 2001. ISSN 0165-1684.

[41] G. Kerschen, K. Worden, A.F. Vakakis, and J.C. Golinval. Past, present and future of nonlinear system identification in structural dynamics. *Mechanical Systems and Signal Processing*, 20(3):505–592, 2006. ISSN 0888-3270.

[42] S. Bellizzi, P. Guillemain, and R. Kronland-Martinet. Identification of coupled non-linear modes from free vibration using time-frequency representations. *Journal of Sound and Vibration*, 243(2):191–213, 2001.

[43] M. Peeters, G. Kerschen, and J.C. Golinval. Phase resonance testing of nonlinear vibrating structures. *Nonlinear Modeling and Applications, Volume 2*, pages 159–169, 2011.

[44] M.O. HINKE. Nonorientable manifolds in three-dimensional vector fields. *International Journal of Bifurcation and Chaos*, 13(03):553–570, 2003.

[45] R.U. Seydel. *Practical bifurcation and stability analysis*, volume 5. Springer, 2009.

[46] J.B. Kuipers. *Quaternions and rotation sequences*. Princeton university press Princeton, NJ, USA:, 1999.

[47] B. Krauskopf and H. Osinga. Two-dimensional global manifolds of vector fields. *Chaos*, 9(3):768–774, 1999.

[48] HM Osinga. Non-orientable manifolds of periodic orbits. In *Proc. Int. Conf. Diff. Eqs*, volume 2, pages 922–924, 2000.

[49] B.A. Dubrovin, A.T. Fomenko, and S.P. Novikov. *Modern geometry: methods and applications. The geometry of surfaces, transformation groups, and fields*. Springer, 1984. ISBN 0387961623.

[50] A. Gray, E. Abbena, and S. Salamon. *Modern differential geometry of curves and surfaces with Mathematica*. Chapman & Hall/CRC, 2006.

[51] J. Guckenheimer and P. Holmes. *Nonlinear oscillations, dynamical systems, and bifurcations of vector fields*. Springer, 2002. ISBN 0387908196.